NUMERICAL TREATMENT FOR 3-D MAGNETIZED CASSON FLUID-FLOW OVER AN UNSTEADY CONVECTIVELY HEATED SURFACE WITH VARIABLE THERMAL CONDUCTIVITY

by

Bhose GANGA[a], Sekar CHARLES[b], Abdul Kaffoor Abdul HAKEEM[c], Manoj Kumar NAYAK[d], Taseer MUHAMMAD[e*], Naura ALBOGAMI[f], and Sivanandam SIVASANKARAN[f]

[a] Department of Mathematics, Providence College for Women, Coonoor, India
[b] Department of Mathematics, PSG College of Arts and Science, Coimbatore, India
[c] Department of Mathematics, SRMV College of Arts and Science, Coimbatore, India
[d] Department of Mechanical Engineering, ITER, Siksha 'O' Anusandhan Deemed to be University, Bhubaneswar, Odisha, India
[e] Department of Mathematics, College of Sciences, King Khalid University, Abha, Saudi Arabia
[f] Mathematical Modelling and Applied Computation (MMAC) Research Group, Department of Mathematics, Faculty of Science, King Abdulaziz University, Jeddah, Saudi Arabia

Original scientific paper
https://doi.org/10.2298/TSCI210611174G

The convective 3-D MHD boundary-layer transport of Casson liquid by an unsteady stretchable sheet set in a permeable medium with variable thermal conductivity is researched. Conservation laws of the mass, the momentum, and the energy are changed into ODE, which are numerically dealt with fourth order Runge-Kutta integration scheme in relationship with shooting procedure. The dimensionless velocity, temperature, skin friction coefficient and the local Nusselt number inside the boundary-layer are processed and examined through graphs and tables for various parameters that portray the flow. The numerical outcomes got for the specific case are sensibly in great concurrence with the existing results.

Key words: *unsteady stretching surface, convective heating process, magnetized Casson fluid, variable thermal conductivity, porous medium, numerical solution*

Introduction

The significance of MHD stream has importance in many designing cycles, for example, peristaltic MHD blower, warm encasings, quickening agents, geothermal frameworks, atomic garbage removal, polymer and oil advances, and plan of cooling frameworks with fluid metals. Each such utilization of MHD gives rise to inspect the issues which incorporate MHD. The MHD are utilized by the authors like Seth *et al.* [1], Murthy *et al.* [2], Sheikholeslami and Shehzad [3], and Sheikholeslami [4]. Especially, the related boundary-layer flows over different surfaces subject to different conditions of motion. Crane [5] developed the closed-form solution for viscous fluid-flow by stretching surface. Later, the Crane's concern has been considered widely from various researchers, Abd El-Aziz and Afify [6], Mabood

* Corresponding author, e-mail: tasgher@kku.edu.sa

and Das [7], Abd El-Aziz and Afify [6], and Thumma *et al.* [9]. In fact, Casson fluid model is a decent one to investigate their properties of non-Newtonian fluids which has been appeared by the investigations in Haldar *et al.* [10], Sivaraj *et al.* [11], Gireesha *et al.* [12], Nayak *et al.* [13], Hamid *et al.* [14], and Hari Krishna *et al.* [15].

All the previously mentioned considers are identified with stream and warmth move qualities over uniform extending surfaces. In any case, for more reasonable portrayal of the stream design, it is essential to incorporate the shakiness into the overseeing conditions of the issue. Wang [16] was the main scientist who examined an insecure limit layer stream of a fluid film over a precarious extending sheet. Irfan *et al.* [17] mathematically dissected the insecure 3-D progression of Carreau nanofluid. Ramadevi *et al.* [18] inspected the impact of thermo diffusion on time subordinate Casson liquid. Trivedi and Ansari [19] examined the temperamental Casson nanoliquid stream in a permeable medium. Kumar and Srinivas [20] explored the impact of Joule warming and warm radiation on shaky hydromagnetic stream of synthetically responding Casson liquid over a slanted permeable extending sheet. Murthy [21], Lakshmietal [22], Reddy *et al.* [23], Nayak *et al.* [24-26] conveyed the influence of various other properties on the flow past an unsteady stretched/shrunk surface.

The convective boundary condition in permeable media has been generally explored tentatively and numerically for a long time because of the numerous essential applications. Regarding this, 3-D MHD flow by Kumar *et al.* [27], effect of variable viscosity, Khan [28], and effect of MHD cross diffusion Ramadevi *et al.* [29] on Casson fluid/nanofluid subject to convective stretched surface have been studied. Related works can also be found from the papers of Nayak *et al.* [30], Kumar *et al.* [31], Raza [32], Nayak *et al.* [33], Raju *et al.* [34], Mabood *et al.* [35], Nayak *et al.* [36], Mahanta and Shaw [37], and Butt *et al.* [38].

A close perception toward this way reveals that so far nobody has developed a numerical model for convective MHD 3-D progression of Casson liquid with variable warm conductivity over an insecure extending surface. Remembering this, an examination has undertaken and the outcomes are plotted and the mathematical results are shown in tables. The significant perceptions of the examination are recorded in the end.

Mathematical formulation

Let us consider 3-D laminar flow of an incompressible Casson fluid by an unsteady stretching surface in a porous medium. The rheological relation for Casson fluid-flow is described by:

$$\tau = \tau_0 + \mu\gamma^* \tag{1}$$

or

$$\tau_{ij} = \begin{cases} 2\left(\mu_B + \dfrac{p_y}{\sqrt{2\pi}}\right)e_{ij}, & \pi > \pi_c \\ 2\left(\mu_B + \dfrac{p_y}{\sqrt{2\pi}}\right)e_{ij}, & \pi < \pi_c \end{cases} \tag{2}$$

The governing expressions for unsteady 3-D flow can be expressed by [37, 38]:

$$\frac{\partial u}{\partial x} + \frac{\partial v}{\partial y} + \frac{\partial w}{\partial z} = 0 \tag{3}$$

$$\frac{\partial u}{\partial t}+u\frac{\partial u}{\partial x}+v\frac{\partial u}{\partial y}+w\frac{\partial u}{\partial z}=\nu\left(1+\frac{1}{\beta}\right)\frac{\partial^2 u}{\partial z^2}-\frac{\sigma B^2(t)}{\rho}u-\frac{\mu_e}{\rho K}u \tag{4}$$

$$\frac{\partial u}{\partial t}+u\frac{\partial u}{\partial x}+v\frac{\partial u}{\partial y}+w\frac{\partial u}{\partial z}=\nu\left(1+\frac{1}{\beta}\right)\frac{\partial^2 v}{\partial z^2}-\frac{\sigma B^2(t)}{\rho}v-\frac{\mu_e}{\rho K}v \tag{5}$$

$$\frac{\partial T}{\partial t}+u\frac{\partial T}{\partial x}+v\frac{\partial T}{\partial y}+w\frac{\partial T}{\partial z}=\frac{1}{\rho C_p}\frac{\partial}{\partial z}\left(k\frac{\partial T}{\partial z}\right)+\frac{16\sigma^* T_\infty^3}{3\rho C_p k^*}\frac{\partial^2 T}{\partial z^2} \tag{6}$$

The corresponding boundary conditions are:

$$u=u_{\mathrm{w}},\quad v=v_{\mathrm{w}},\quad w=0,\quad -k\frac{\partial T}{\partial z}=h_{\mathrm{f}}(T_{\mathrm{f}}-T),\quad \text{at } z=0$$

$$u\to 0,\quad v\to 0,\quad T\to T_\infty \text{ as } z\to\infty \tag{7}$$

We consider the specific model for variable thermal conductivity:

$$k=k_\infty\left(1+\varepsilon\frac{T-T_\infty}{\Delta T}\right)$$

where ε is the thermal conductivity parameter. This relation can be written as $k=k_\infty(1+\varepsilon\theta)$, see Irfan *et al.* [17]. Further, $u_{\mathrm{w}}=ax/(1-\gamma t)$ and $v_{\mathrm{w}}=by/(1-\gamma t)$ are stretching velocities. Following the transformations, Butt [38]:

$$\left.\begin{aligned} u=\frac{ax}{1-\gamma t}f'(\eta),\quad v=\frac{ay}{1-\gamma t}g'(\eta),\quad \eta=z\sqrt{\frac{a}{\nu(1-\gamma t)}}\\ w=\sqrt{\frac{a\nu}{1-\gamma t}}[f(\eta)+g(\eta)],\quad \theta(\eta)=\frac{T-T_\infty}{T_{\mathrm{f}}-T_\infty}\end{aligned}\right\} \tag{8}$$

In view of eq. (8), eq. (3) is identically verified and eqs. (4)-(6) yield:

$$\left(1+\frac{1}{\beta}\right)f'''+(f+g)f''-f'^2-A\left(f'+\eta\frac{f''}{2}\right)-(\mathrm{M}+\lambda)f'=0 \tag{9}$$

$$\left(1+\frac{1}{\beta}\right)g'''+(f+g)g''-g'^2-A\left(g'+\eta\frac{g''}{2}\right)-(\mathrm{M}+\lambda)g'=0 \tag{10}$$

$$(1+\varepsilon\theta+R)\theta''+\varepsilon\theta'^2+\mathrm{Pr}(f+g)\theta'-\frac{A}{2}\eta\theta'=0 \tag{11}$$

The boundary conditions are written:

$$\left.\begin{aligned} f(0)+g(0)=0,\quad f'(0)=1,\quad g'(0)=\frac{b}{a}=\alpha,\\ \theta'(0)=-B_i[1-\theta(0)] \text{ at } \eta=0\\ f'(\infty)\to 0,\quad g'(\infty)\to 0,\quad \theta(\infty)\to 0 \text{ as } \eta\to\infty\end{aligned}\right\} \tag{12}$$

One can set:

$$f(0) = g(0) = 0 \tag{13}$$

Here,

$$\begin{gathered} A = \frac{\gamma}{a}, \quad \mathrm{M} = \frac{\sigma^* B_0^2}{\rho a}, \quad \lambda = \frac{\mu}{\rho\nu}\frac{\mathrm{Re}_x}{\mathrm{Re}_k^2}, \quad \mathrm{Re}_x = \frac{u_\mathrm{w} x}{\nu}, \\ \mathrm{Re}_k = \frac{u_w\sqrt{K}}{\nu}, \quad \alpha = \frac{b}{a}, \quad \mathrm{Pr} = \frac{\rho\nu C_p}{k}, \quad R = \frac{16\sigma^* T_\infty^3}{3kk^*}, \quad \mathrm{Bi} = \frac{h_\mathrm{f}}{k}\sqrt{\frac{\nu}{a}} \end{gathered} \tag{14}$$

The non-dimensional wall shear-stress and wall heat-flux are respectively:

$$\mathrm{Re}_x^{1/2} C_{\mathrm{f}x} = \left(1 + \frac{1}{\beta}\right) f''(0), \quad \mathrm{Re}_y^{1/2} C_{\mathrm{f}y} = \left(1 + \frac{1}{\beta}\right) g''(0), \quad \mathrm{Re}_x^{-½}\,\mathrm{Nu}_x = -\theta'(0) \tag{15}$$

Numerical procedure

The system of eqs. (9)-(11) subject to boundary conditions (12) is computed by using forth-order Runge-Kutta method with a shooting technique. Letting:

$$\begin{gathered} y_2 = f' \\ y_3 = y_2' = f'' \\ y_5 = g' \\ y_6 = y_5' = g'' \\ y_8 = \theta' \end{gathered}$$

Then the equivalent forms of eqs. (9)-(11) under the new variable is:

$$\begin{gathered} y_1' = y_2 \\ y_2' = y_3 \\ y_3' = \frac{y_2^{\,2} - (y_1 + y_4)y_3 + A\left(y_2 + \frac{\eta}{2}y_3\right) + (\mathrm{M} + \lambda)y_2}{\left(1 + \frac{1}{\beta}\right)} \\ y_4' = y_5 \\ y_5' = y_6 \\ y_6' = \frac{y_5^{\,2} - (y_1 + y_4)y_6 + A\left(y_5 + \frac{\eta}{2}y_6\right) + (\mathrm{M} + \lambda)y_5}{\left(1 + \frac{1}{\beta}\right)} \\ y_7' = y_8 \\ y_8' = \frac{A\mathrm{Pr}\frac{\eta}{2}y_8 - \mathrm{Pr}[(y_1 + y_4)y_8] - \varepsilon y_8^{\,2}}{(1 + \varepsilon y_7 + R)} \end{gathered} \tag{16}$$

the corresponding boundary condition in new variables are given:

$$\begin{aligned} y_1 &= 0 \\ y_2 &= 1 \\ y_3 &= \text{unknown} \\ y_4 &= o \\ y_5 &= \alpha \\ y_6 &= \text{unknown} \\ y_7 &= \text{unknown} \\ y_8 &= -B_i(1-y_7) \end{aligned} \tag{17}$$

Now to solve the initial value problem (16), we need the values for $y_3(0)$, $y_6(0)$, *i.e.* $f'''(0)$, $g''(0)$, and $y_7(0)$, *i.e.* $\theta(0)$. But no such values are known in advance.

In this method we have to choose $\eta \to \infty$, which is satisfied at a finite value, say η_∞. The guess for $f''(0), g''(0),$ and $\theta(0)$ have been taken and fourth-order Runge-Kutta technique is employed to get the solution. Then we compared the estimations of $f'(\eta), g'(\eta),$ and $\theta(\eta)$ with the boundary conditions and are adjusted using shooting iteration technique for better approximation. Step size $\Delta\eta = 0.001$ is considered to get the numeric simulation and exactness to fifth decimal place is picked as convergence criterion.

Discussion and validation

In this section we discuss the indicators of the characteristics: the velocity, temperature, sheath friction coefficient, and local Nusselt number profiles for varied estimations of unsteadiness parameter A, the stretching parameter α, the Casson parameter β, the porosity parameter λ, the magnetic parameter M, the Biot number Bi, the variable thermal conductivity parameter ε, the radiation parameter R, and the Prandtl number Pr, and they are presented by well-structured graphs and numerically computed tables.

In general, the values of the parameters are fixed as follows: $A = 2.2$, $\alpha = 0.5$, $\beta = 1.5$, $\lambda = 2.0$, M = 1.0, Bi = 5.0, $\varepsilon = 0.7$, $R = 1$, Pr = 0.9. When compared our results with Butt *et al.* [38] in tab. 1, it appears to have come around to the view that increase in α upsurges the absolute value of $f''(0), g''(0)$ in the present result and the results of Butt [38]. It is remarkable here to mention that our results are very close to the results of Butt [38] and therefore in excellent agreement with it, see tab. 1. Same aspects are visualized for different estimations of λ, see tab. 2.

Table 1. Comparison of results for $f''(0)$ and $g''(0)$ for different values of α when M = 0, λ = 0, and $\beta \to \infty$

α	[38]		Present results	
	$-f''(0)$	$-g''(0)$	$-f''(0)$	$-g''(0)$
0.0	1	0	1	0
0.1	1.020260	0.066847	1.02025978	0.06684715
0.2	1.039495	0.148737	1.03949519	0.14873691
0.3	1.057955	0.243360	1.05795478	0.24335980
0.4	1.075788	0.349209	1.07578811	0.34920865
0.5	1.093095	0.465205	1.09309502	0.46520485

Table 2. Comparison of results for $f''(0)$ for different values of λ when M = 0, α = 0, A = 0.5, and $\beta \to \infty$

λ	[38]	Present results
	$-f''(0)$	$-f''(0)$
0.0	1.167212	1.16721163
0.5	1.366237	1.36623757
1.0	1.539051	1.53905159
1.5	1.694085	1.69408510
2.0	1.835962	1.83596217

Velocity profile manifestation

In this analysis, fig. 1 portrays the axial as well as transverse velocity for various estimations of A. Here, it is demonstrated that undergoing a continuous change, the A makes diminution of the velocity profile. With an expansion of A the velocities $f'(\eta)$ and $g'(\eta)$ diminish together with a reduction in the thickness of the respective momentum boundary-layers. The very cause of such diminution is due to less stretching of the surface. In further part of the analysis, fig. 2 depicts effect of α on $f'(\eta)$ and $g'(\eta)$, respectively. Greater estimations of α shows higher stretching rate along y-direction compared to x-direction. Thus with an increment in α, velocity in y-direction enlarges while it shows opposite behavior in x-direction. The effect of β on $f'(\eta)$ and $g'(\eta)$ is illustrated in fig. 3. We take note of that with amplifying β, the velocities $f'(\eta)$ and $g'(\eta)$ and the respective boundary-layer thickness get diminution which is due to an increment in the fluid resistance. It is likewise watched that the magnitude of the axial velocity is greater than that of transverse velocity. A diagram showing the relation between variable quantities of porosity parameter and the flow fields $f'(\eta)$ and $g'(\eta)$ has been illustrated in fig. 4. It elucidates that for growing λ, the velocities $f'(\eta)$ and $g'(\eta)$ decline as a result of resistive force offered by the porous medium. Figure 5 delineates the impact of M on $f'(\eta)$ and $g'(\eta)$. The increasing M diminishes $f'(\eta)$ and $g'(\eta)$ prompting descending velocity boundary-layer thickness. The Lorentz force which is having control over the fluid motion emerges due to the connected transverse magnetic field, and is being the primary cause for lessening the fluid velocity.

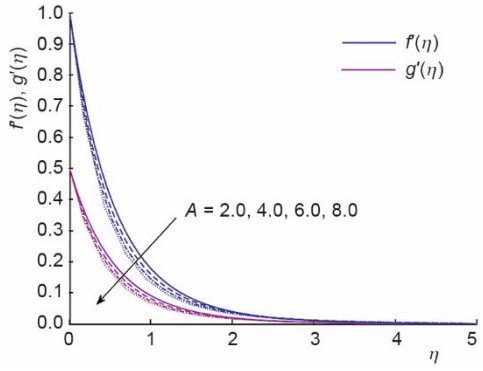

Figure 1. Effects of A on $f'(\eta)$ and $g'(\eta)$ when β = 1.5, λ = 2.0, and α = 0.5

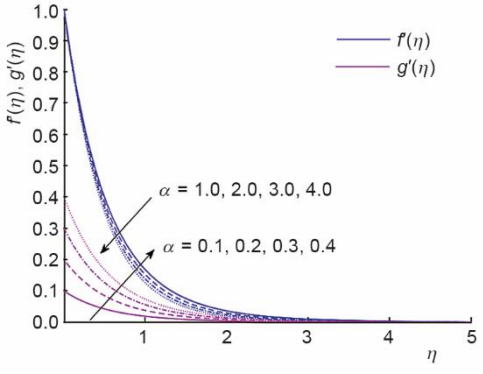

Figure 2. Effects of α on $f'(\eta)$ and $g'(\eta)$ when β = 1.5, λ = 2.0, M = 1.0, and A = 2.2

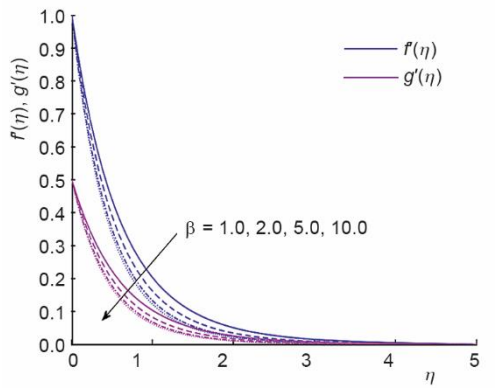

Figure 3. Effects of β on $f'(\eta)$ and $g'(\eta)$ when α = 0.5, λ = 2.0, M = 1.0, and A = 2.2

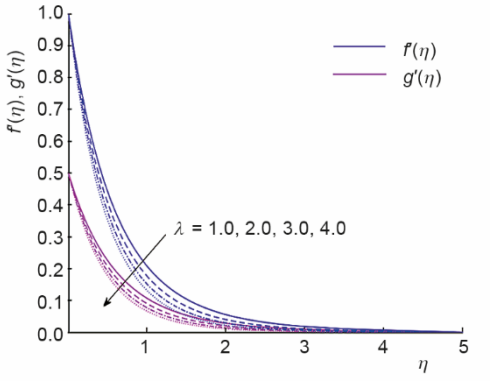

Figure 4. Effects of λ on $f'(\eta)$ and $g'(\eta)$ when β = 1.5, α = 0.5, M = 1.0, and A = 2.2

Temperature profile manifestation

Figure 6 is shown to examine impacts of A and β on temperature $\theta(\eta)$. The escalating values of β improves $\theta(\eta)$ and the related thermal boundary-layer thickness. Increasing β declines the fluid velocity by decreasing the yield stress. Thus the rate of heat transportation is impressively enhanced by an expansion of β. Meanwhile the temperature curves in fig. 6 magnify due to rise in A. More heat is dragged from the sheet to the fluid when A hikes. For this reason $\theta(\eta)$ increases. Figure 7 is sketched to see the impact of α and λ on $\theta(\eta)$. It is understood that $\theta(\eta)$ and furthermore the thermal boundary-layer thickness diminish with increasing α. Furthermore, rise in λ augments both the temperature as well as the thermal boundary-layer thickness. Figure 8 exhibits the temperature profiles for different estimations of ε and Bi. Here $\theta(\eta)$ profiles get intensified when we amplify Bi. In fact, Bi creates profound convection so that its higher values generates the higher $\theta(\eta)$ profiles and more thermal boundary-layer thickness. From the same plot we visualize that the amplified estimation of thermal conductivity parameter ϵ, $\theta(\eta)$ diminishes. Figure 9 narrates that the rise in magnetic field strength upsurges $\theta(\eta)$ and the thermal boundary-layer thickness. In the same plot it is noticed that the increment in R peters out $\theta(\eta)$ in the boundary-layer region. More radiation from the fluid indicates that more loss of heat from it thereby loosing temperature.

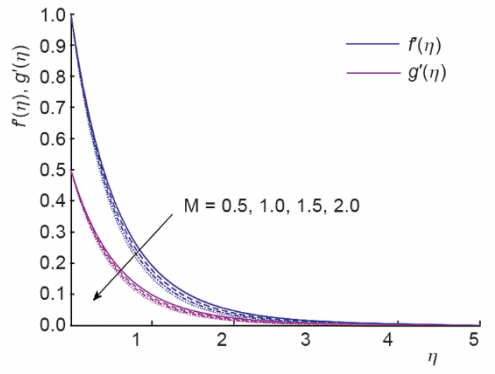

Figure 5. Effects of M on $f'(\eta)$ and $g'(\eta)$ when β = 1.5, α = 0.5, λ = 2.0, and A = 2.2

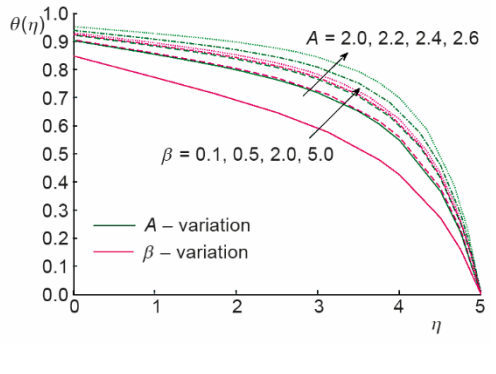

Figure 6. Effects of A and β on $\theta(\eta)$ when α = 0.5, λ = 2.0, ε = 0.7, M = 1.0, Bi = 5.0, R = 1.0, and Pr = 0.9

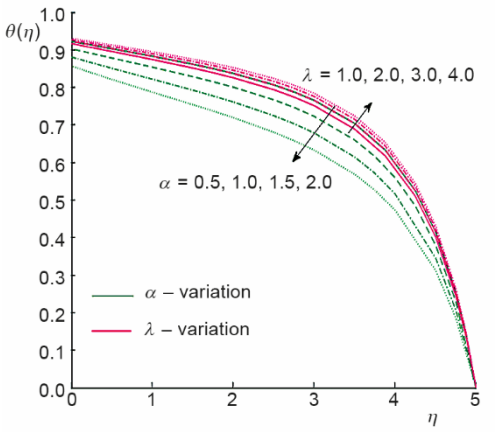

Figure 7. Effects of α and λ on $\theta(\eta)$ when A = 2.2, β = 1.5, ε = 0.7, M = 1.0, Bi = 5.0, R = 1.0, and Pr = 0.9

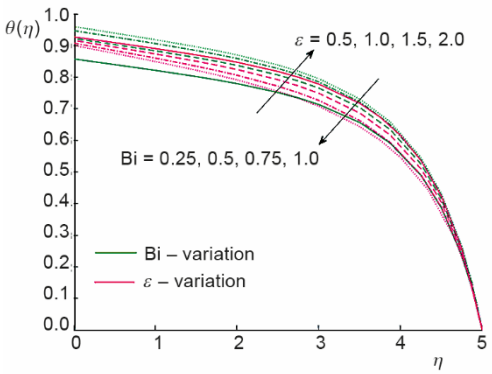

Figure 8. Effects of Bi and ε on $\theta(\eta)$ when A = 2.2, β = 1.5, λ = 2.0, M = 1.0, α = 0.5, R = 1.0, and Pr = 0.9

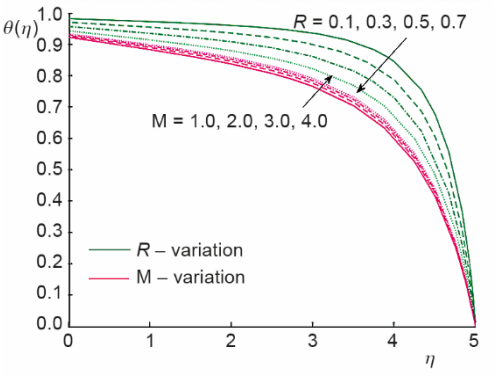

Figure 9. Effects of R and M on $\theta(\eta)$ when A = 2.2, β = 1.5, λ = 2.0, Bi = 5.0, α = 0.5, ε = 0.7, and Pr = 0.9

Skin friction profiles manifestation

Figures 10-14 are depicted to visualize impacts of different physical numbers on axial skin-friction coefficient:

$$\left\{-\left(1+\frac{1}{\beta}\right)f''(0)\right\}$$

and transverse skin-friction coefficient:

$$\left\{-\left(1+\frac{1}{\beta}\right)g''(0)\right\}$$

Figsures 10 and 11 show the effects of α and A on:

$$\left\{-\left(1+\frac{1}{\beta}\right)f''(0)\right\} \quad \text{and} \quad \left\{-\left(1+\frac{1}{\beta}\right)g''(0)\right\}$$

A comparison of figs. 10 and 11 show that both skin friction coefficients decay with rise in α. In accordance with fig. 12, the surface viscous drag:

$$\left\{-\left(1+\frac{1}{\beta}\right)f''(0)\right\} \quad \text{and} \quad \left\{-\left(1+\frac{1}{\beta}\right)g''(0)\right\}$$

diminish for varied estimations of β and A. It is obvious from fig. 13 that the bigger values of λ lower both:

$$\left\{-\left(1+\frac{1}{\beta}\right)f''(0)\right\} \quad \text{and} \quad \left\{-\left(1+\frac{1}{\beta}\right)g''(0)\right\}$$

A similar kind of result is accomplished for different M in fig. 14. In all the mentioned figures transverse surface viscous drag:

$$\left\{-\left(1+\frac{1}{\beta}\right)g''(0)\right\}$$

is of greater magnitude than axial surface viscous drag:

$$\left\{-\left(1+\frac{1}{\beta}\right)f''(0)\right\}$$

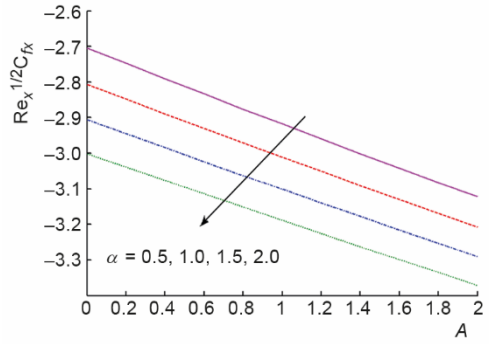

Figure 10. The $\mathrm{Re}_x^{1/2}C_{fx}$ for different α and A when λ = 2.0, Bi = 5.0, β = 1.5, ε = 0.7, M = 1.0, R = 1.0, and Pr = 0.9

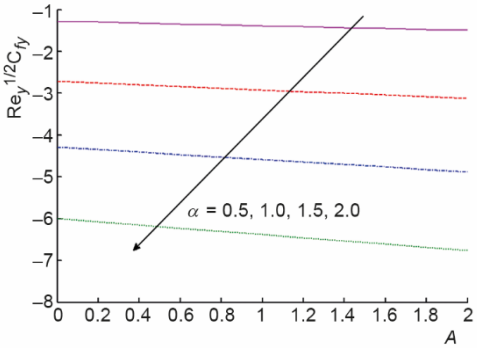

Figure 11. The $\mathrm{Re}_y^{1/2}C_{fy}$ for different α and A when λ = 2.0, Bi = 5.0, β = 1.5, ε = 0.7, M = 1.0, R = 1.0, and Pr = 0.9

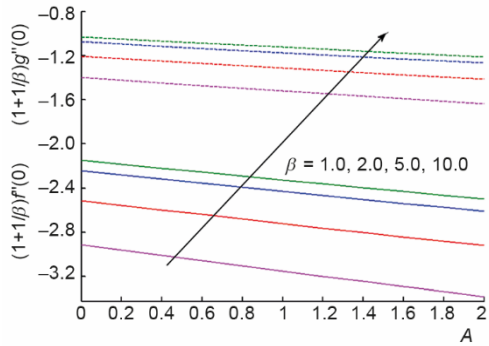

Figure 12. The $(1 + 1/\beta)f''(0)$ and $(1 + 1/\beta)g''(0)$ for different β and A when λ = 2.0, Bi = 5.0, α = 0.5, ε = 0.7, M = 1.0, R = 1.0, and Pr = 0.9

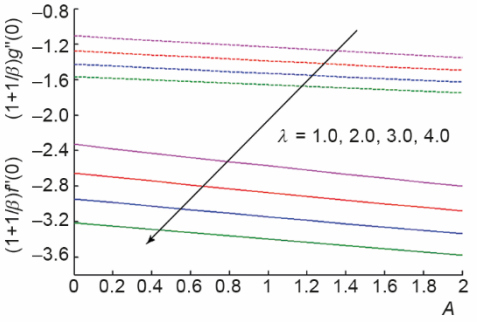

Figure 13. The $(1 + 1/\beta)f''(0)$ and $(1 + 1/\beta)g''(0)$ for different λ and A when β = 1.5, Bi = 5.0, α = 0.5, ε = 0.7, M = 1.0, R = 1.0, and Pr = 0.9

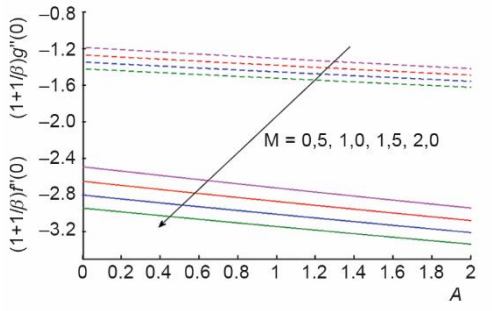

Figure 14. The $(1 + 1/\beta)f''(0)$ and $(1 + 1/\beta)g''(0)$ for different M and A when β = 1.5, Bi = 5.0, α = 0.5, ε = 0.7, R = 1.0, and Pr = 0.9

Nusselt number profile manifestation

At the beginning, fig. 15 reveals that Nusselt number:

$$\left\{\mathrm{Re}_x^{-\frac{1}{2}}\,\mathrm{Nu}_x\right\}$$

decays with the rise in β. The rate of heat transportation decreases due to hike in λ, fig. 16. Further, heat transfer rate from the stretched surface augments with increase in Bi, fig. 17. The rate of heat transportation declines for rise in ε, see fig. 18. Figsures 19 and 20 indicate that heat transfer rate gets diminution for rise in M and R. However, rise in Pr exhibits exactly opposite effect on:

$$\left\{\mathrm{Re}_x^{-\frac{1}{2}}\,\mathrm{Nu}_x\right\}$$

(see fig. 21). From tab. 3, it is obtained the variation of heat transfer rate $\{-\theta'(0)\}$ for varied estimations of A, α, β, λ, M, Bi, ε, and R. It is observed that heat transfer rate $\{-\theta'(0)\}$ peters out for rise in A, β, λ, M, and ε while reverse trend is the result in respect of hike in α, Bi, R.

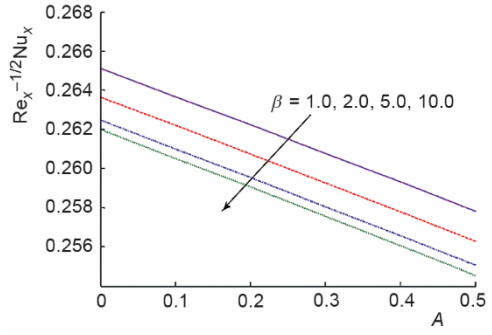

Figure 15. The $\mathrm{Re}_x^{-1/2}\mathrm{Nu}_x$ for different β and A when λ =2.0, M = 1.0, Bi = 5.0, α = 0.5, ε = 0.7, R = 1.0, and Pr = 0.9

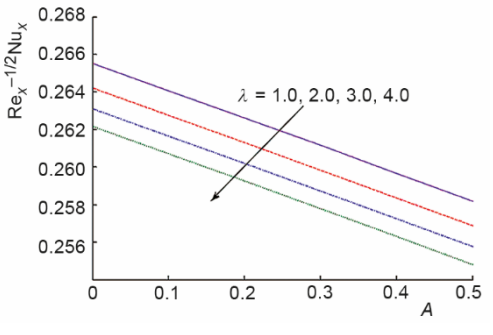

Figure 16. The $\mathrm{Re}_x^{-1/2}\mathrm{Nu}_x$ for different λ and A when β = 1.5, α = 0.5, Bi = 5.0, M = 1.0, ε = 0.7, R = 1.0, and Pr = 0.9

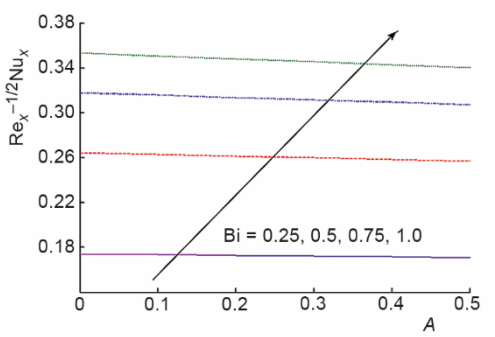

Figure 17. The $Re_x^{-1/2}Nu_x$ for different Bi and A when β = 1.5, λ = 2.0, α = 0.5, M = 1.0, ε = 0.7, R = 1.0, and Pr = 0.9

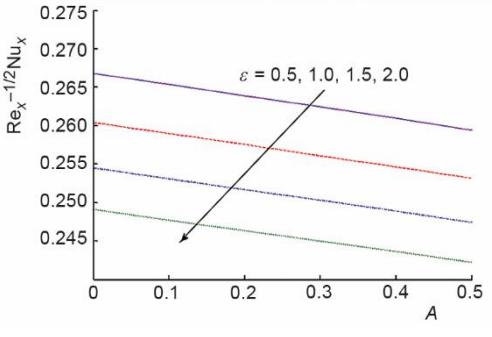

Figure 18. The $Re_x^{-1/2}Nu_x$ for different ε and A when β = 1.5, λ = 2.0, α = 0.5, M = 1.0, ε = 0.7, R = 1.0, and Pr = 0.9

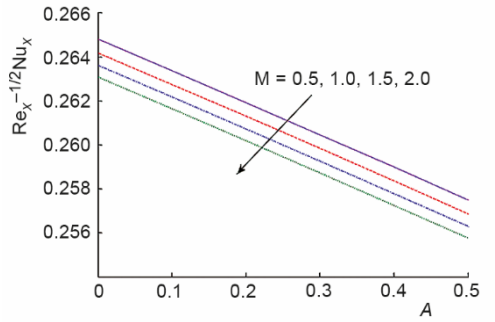

Figure 19. The $Re_x^{-1/2}Nu_x$ for different M and A when β = 1.5, λ = 2.0, α = 0.5, Bi = 5.0, ε = 0.7, R = 1.0, and Pr = 0.9

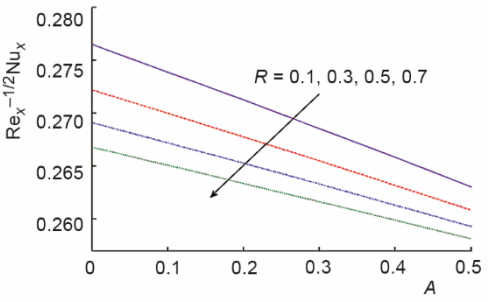

Figure 20. The $Re_x^{-1/2}Nu_x$ for different R and A when β = 1.5, λ = 2.0, α = 0.5, M = 1.0, ε = 0.7, Bi = 5.0, and Pr = 0.9

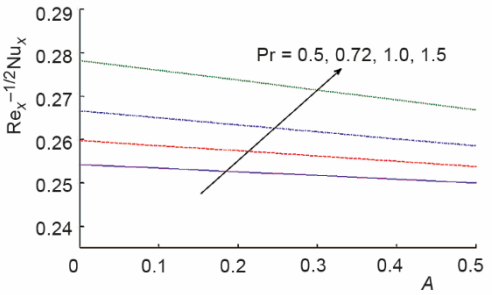

Figure 21. The $Re_x^{-1/2}Nu_x$ for different Pr and A when β = 1.5, λ = 2.0, α = 0.5, M = 1.0, ε = 0.7, R = 1.0, and Bi = 5.0

Table 3. Values of Nusselt number for various estimations of physical parameters

A	α	β	λ	M	Bi	ε	R	Pr	$-\theta'(0)$
0.1									0.47289707
0.2									0.46828722
0.3									0.46367995
	1.0								0.39689824
	2.0								0.43433661
	3.0								0.47022120
		1.0							0.38043921
		2.0							0.37583439
		5.0							0.37221670
			1.0						0.38082903
			2.0						0.37753352
			3.0						0.37473275
				0.5					0.37911083
				1.0					0.37753352
				1.5					0.37607916
					0.5				0.22953004
					0.75				0.26916828
					1.0				0.29432728
						0.5			0.38666381
						1.0			0.36573850
						1.5			0.34993454
							0.1		0.32330287
							0.3		0.34090226
							0.5		0.35444160
								0.5	0.39184063
								1.0	0.37393555
								1.5	0.35585298

Conclusions

Convective 3-D MHD boundary-layer flow of Casson fluid over an unsteady stretching sheet in a porous medium with variable thermal conductivity is discussed. The velocity $f'(\eta)$ diminishes for rise in α, whereas $g'(\eta)$ upsurges. The fluid-flow gets diminution in the presence of rise in A, M, λ, and β. The increase in A, M, λ, and β, Bi and Pr leads to growth of $\theta(\eta)$ while that of α, ε, and R undermines it. The magnitude of:

$$\left\{-\left(1+\frac{1}{\beta}\right)f''(0)\right\} \quad \text{and} \quad \left\{-\left(1+\frac{1}{\beta}\right)g''(0)\right\}$$

decreases due to increase in β and contributes opposite effect for α, λ, and M. The heat transfer rate was found to be higher for increment in α, Bi, R, while it became lower for rise in A, β, λ, M, ε, and Pr.

Acknowledgment

The Deanship of Scientific Research (DSR) at King Abdulaziz University (KAU), Jeddah, Saudi Arabia has funded this project, under grant no. (KEP-PhD: 96-130-1443).

Nomenclature

A – unsteadiness parameter
a, b – rate constants, [s^{-1}]
Bi – Biot number
B_0 – strength of uniform magnetic field, [Tesla]
e_{ij} – $(i, j)^{th}$ component of the deformation rate, [s^{-1}]
ρC_p – specific heat capacity of fluid, [$Jkg^2m^3K^{-1}$]
h_f – convective heat transfer coefficient, [$Calm^{-2}s^{-1}K^{-1}$]
k_f – thermal conductivity, [$Wm^{-1}K^{-1}$]
k^* – mean absorption coefficient, [m^{-1}]
K – porous medium permeability, [m^2]
M – Hartmann number
Pr – Prandtl number
p_y – yield stress, [Nm^{-2}]
R – thermal radiation parameter
Re – Reynolds number
T – temperature of the fluid [K]
T_w – temperature of the fluid on the wall, [K]
T_∞ – ambient fluid temperature, [K]
T_f – temperature for convective heating, [K]
ΔT – temperature difference, [K]
$\mathrm{Re}_x^{1/2} C_{fx}$ – local axial skin friction coefficient
$\mathrm{Re}_y^{1/2} C_{fy}$ – local transverse skin friction coefficient
$\mathrm{Re}_x^{-1/2} \mathrm{Nu}_x$ – local Nusselt number
(u, v, w) – fluid velocity components along (x, y, z) directions, [ms^{-1}]

Subscripts

f – fluid
w – quantities at wall
∞ – quantities at free stream

Greek symbols

α – velocity ratio parameter
β – Casson fluid parameter
λ – porosity parameter
η – shear stress
μ – dynamic viscosity of fluid, [$kgm^{-1}s^{-2}$]
μ_B – dynamic viscosity of viscoplastic fluids, [$kgm^{-1}s^{-1}$]
π – product of the component of deformation rate itself, [s^{-2}]
π_c – critical value based on the type of non-Newtonian model
ρ – density of fluid, [kgm^{-3}]
σ – electrical conductivity, [S/m]
σ^* – Stefan Boltzmann constant, [$Wm^{-2}K^{-4}$]
ν – kinematic viscosity, [m^2s^{-1}]

References

[1] Seth, G. S., *et al.*, Double Diffusive MHD Casson Fluid-flow in a Non-Darcy Porous Medium with Newtonian Heating and Thermo-Diffusion Effects, *Int. J. Heat and Technol., 36* (2018), 4, pp. 1517-1527
[2] Murthy, M. K., *et al.,* Magnetohydrodynamic Boundary-layer Slip Casson Fluid-flow over a Dissipated Stretched Cylinder, *Defect and Diffusion Forum, 393* (2019), June, pp. 73-82
[3] Sheikholeslami, M., Shehzad, S. A., Magnetohydrodynamicnanofluidconvective Flow in a Porous Enclosure by Means of LBM, *Int. J. Heat Mass Transf., 113* (2017), Mar., pp. 796-805
[4] Sheikholeslami, M., Magnetohydrodynamicnanofluid Forced Convection in a Porous Lid Driven Cubic Cavity Using Lattice Boltzmann Method, *Journal of Mol. Liq., 231* (2017), Apr., pp. 555-565
[5] Crane, L. J., Flow Past a Stretching Plate, Z. Angew, *Math.Physk., 21* (1970), July, pp. 645-647
[6] AbdEl-Aziz, M., Afify, A. A., MHDCasson Fluid-flow Over a Stretching Sheet with Entropy Generation Analysis and Hall Influence, *Entropy, 21* (2019), 6, 592

[7] Mabood, F., Das, K., Outlining the Impact of Melting on MHD Casson Fluid-flow Past a Stretching Sheet in A Porous Medium with Radiation, *Heliyon, 5* (2019), 2, e01216
[8] Abd El-Aziz, M., Afify, A. A., Influences of Slip Velocity and Induced Magnetic Field on MHD Stagnation-Point Flow and Heat Transfer of Casson Fluid Over a Stretching Sheet, *Math. Probl. Eng.*, *2018* (2018), ID 9402836
[9] Thumma, T., *et al.,* Effect of Heat Generation and Viscous Dissipationon MHD 3-D Cassonnanofluid-flow Past an Impermeable Stretching Sheet, in: *Num. Heat Transf. Fluid-flow, Lecture Notes in Mechanical Eng.,* Springer, Singapore, 2019, pp. 575-585
[10] Haldar, S., *et al.,* Flow and Heat Transfer of Casson Fluid Over an Exponentially Shrinking Permeable Sheet in Presence of Exponentially Moving Free Stream with Convective Boundary Condition, *Mechanics of Advanced Materials and Structures, 26* (2019), 17, pp. 1498-1504
[11] Sivaraj, R., *et al.,* Investigation of Cross-Diffusion Effects on Casson Fluid-flow in Existence of Variable Fluid Properties, *The Eur. Physical J. Spec. Topics, 228* (2019), 1, pp. 35-53
[12] Gireesha, B. J., *et al.,* Exploration of Activation Energy and Binary Chemical Reaction Effects on Nanocasson Fluid-flow with Thermal and Exponential Space-Based Heat Source, *Multidiscipline Modeling in Materials and Structures, 15* (2019), 1, pp. 227-245
[13] Nayak, M. K., *et al.,* 3-D Bioconvective Multiple Slip Flow of Chemically Reactive Cassonnanofluid with Gyrotactic Microorganisms, *Heat Transf. Asian Res., 49* (2020), 1, pp. 135-153
[14] Hamid, M., *et al.,* Dualsolutions and Stability Analysis of Flow and Heat Transfer of Casson Fluid Over a Stretching Sheet, *Physics Letters A, 383* (2019), 20, pp. 2400-2408
[15] Hari Krishna, Y., *et al.,* Chemical Reaction Effect on MHD Flow of Casson Fluid with Porous Stretching Sheet, *Defect and Diffusion Forum, 389* (2018), Nov., pp. 100-109
[16] Wang, C. Y., Liquid Film on an Unsteady Stretching Surface, *Quart. Appl. Math., 48* (1990), Dec., pp. 1234-1237
[17] Irfan, M., *et al.,* Numerical Analysis of Unsteady 3-D Flow of Carreaunanofluid with Variable Thermal Conductivity and Heat Source/Sink, *Results in Phy., 7* (2017), Aug., pp. 3315-3324
[18] Ramadevi, B., Influence of Thermodiffusion on Time Dependent Casson Fluid-flow Past a Wavy Surface, *Int. J. Math. Eng. Management. Sci., 3* (2018), 4, pp. 472-490
[19] Trivedi, M., Ansari, M. S., Unsteady Casson Fluid-flow in a Porous medium with Inclined Magnetic Field in Presence of Nanoparticles, *Eur. Phys. J. Spec. Top. 228*, (2019), Dec., pp. 2553-2569
[20] Kumar, C. K., Srinivas, S., Influence of Joule Heating and Thermal Radiation on Unsteady Hydromagnetic Flow of Chemically Reacting Casson Fluid Over an Inclined Porous Stretching Sheet, *Special Topics & Reviews in Porous Media: An Int. J., 10* (2019), 4, pp. 385-400
[21] Murthy, M. K., MHD Three Dimensional Flow of Casson Fluid Over an Unsteady Exponentially Stretching Sheet with Slip Conditions, *Defect and Diffusion Forum, 388* (2018), Oct., pp. 77-95
[22] Lakshmi, B., *et al.,* Effect of Suction/Blowing on Unsteady MHD Slip Flow of Casson Fluid Over a Stretching Sheet with Thermal Radiation, *J. Sci. Arts, 2* (2018), 43, pp. 503-514
[23] Suresh Reddy, E., *et al.,* Cross Flow on Transient Double - Diffusive Natural Convection in Inclined Porous Trapezoidal Enclosures, *Heat Transf., 50* (2021), 1, pp. 1-27
[24] Nayak, M. K., *et al.,* Influence of Relaxation - Retardation Viscous Dissipation on Chemically Reactive Flow of Oldroyd-B Nanofluid with Hyperbolic Boundary Conditions, *Heat Transf., 49* (2020), 8, pp. 4945-4967
[25] Nayak, M. K., *et al.,* Entropy Optimized MHD 3-D Nanomaterial of Non-Newtonian Fluid: A Combined Approach to Good Absorber of Solar Energy and Intensification of Heat Transport, *Comp. Meth. Prog. Biomed., 186* (2020), Apr., 105131
[26] Nayak, M. K., *et al.,* Time Varying Chemically Reactive MHD Non-Linear Falkner-Skan Flow Over a Permeable Stretching/Shrinking Wedge: Buongiorno Model, *J. Nanofluids, 8* (2019), 3, pp. 467-476
[27] Kumar, P. V., *et al.,* The Studyof Threedimensional Radiative MHDC Asson Nanofluid Over an Exponential Porous Stretching Sheet with Heat Source Under Convective Boundary Conditions, *Int. J. of Heat Technol., 36* (2018), 1, pp. 1-10
[28] Khan, M., Heat and Mass Diffusions for Casson Nanofluid-flow Over a Stretching Surface with Variable Viscosity and Convective Boundary Conditions, *J. Brazilian Society Mech. Sci. Eng., 40* (2018), 11, pp. 1-10
[29] Ramadevi, B., *et al.,* Cross-Diffusion Effects on MHD Cattaneo-Christov Flow of Casson Fluid Past a Convective Linear/Non- Linear Stretching Sheet, *Defect and Diffusion Forum, 388* (2018), Oct., pp. 96-113

[30] Nayak, M. K., *et al.,* Flow and Thermal Analysis on Darcy-Forchheimer Flow of Copper-Water Nanofluid Due to a Rotating Disk: A Static and Dynamic Approach, *J. mater. Res. technol., 9* (2020), 4, pp. 7387-7408
[31] Kumar, G., *et al.,* Cross Diffusion Effect on MHD Mixed Convection Flow of Non-Linearr adiative Heat and Mass Transfer of Casson Fluid Over a Vertical Plate, *Results in Phys., 8* (2018), Mar., pp. 694-701
[32] Raza, J., Thermal Radiation and Slip Effects on Magnetohydrodynamic (MHD) Stagnation Point Flow of Casson Fluid Over a Convective Stretching Sheet, *Propulsion and Power Research, 8* (2019), 2, pp. 138-146
[33] Nayak, M. K., *et al.,* Combined Effects of Slip and Convective Boundary Condition on MHD 3-D Stretched Flow of Nanofluid Through Porous Media Inspired by Non-Linear Thermal Radiation, *Indian J. Phy., 92* (2018), 87, pp. 1017-1028
[34] Raju, C. S. K., *et al.,* MHD Casson Fluid in a Suspension of Convective Conditions and Cross Diffusion Across a Surface of Paraboloid of Revolution, *Alexandria Eng. J., 57* (2018), 4, pp. 3615-3622
[35] Mabood, F., *et al.,* EMHD Flow of Non-Newtonian Nanofluids Over thin Needle with Robinson's Condition and Arrhenius Pre-Exponential Factor Law, *Phys. Scr., 95* (2020), 11, 115219
[36] Nayak, M. K., MHD 3-D Flow and Heat Transfer Analysis of Nanofluid by Shrinking Surface Inspired by Thermal Radiation and Viscous Dissipation, *Int. J. Mech. Sci., 125* (2017), May, pp. 185-193
[37] Mahanta, G., Shaw, S., 3-D Casson Fluid-flow Past a Porous Linearly Stretching Sheet with Convective Boundary Condition, *Alexandria Eng. J., 54* (2015), 3, pp. 653-659
[38] Butt, A. S., *et al.,* Three-Dimensional Flow of a Magnetohydrodynamiccasson Fluid Over an Unsteady Stretching Sheet Embedded into a Porous Medium, *J. Appl. Mechanics Techn. Phy., 57* (2016), 2, pp. 283-292

Paper submitted: June 11, 2021
Paper revised: May 16, 2022
Paper accepted: June 4, 2022